Arch. Metall. Mater. **68** (2023), 1, 37-42

DOI: https://doi.org/10.24425/amm.2023.141469

CHUNXUE WEI[1*], HONGBING LI[1]

PROPERTIES OF Ni60/SiO_2 COATING PREPARED BY THE PYROLYSIS PRODUCTS OF RICE HUSK

Surface coating technology, as the main technology to improve the fatigue life of mechanical systems, has been well applied in mechanical equipment. The present study aimed to explore low-cost surface coating preparation technology using inexpensive rice husk as the research object, and the pyrolysis process behavior of rice husk was analyzed. The Ni60/SiO_2 coating was prepared on the surface of the 45# steel substrate using the pyrolysis product SiO_2 fiber as the reinforcing phase and supersonic plasma-spraying equipment. The results showed no defects such as cracks, pores, and inclusions in the prepared coating. The nanohardness of the Ni60/SiO_2 coating reached 6506 μN, and the average friction coefficient reached 0.42. In the friction-and-wear experiment, the Ni60/SiO_2 coating was manifested as an abrasive wear mechanism.

Keywords: Ni60/SiO_2; Coating; Rice husk; Hardness; Wear

1. Introduction

China is the world's largest rice-growing country (accounting for more than 30% of the total global rice output), and hence the largest producer of rice husks, with an annual output of more than 40 million tons [1,2]. Dealing with these huge amounts of agricultural waste is an urgent issue that needs immediate attention [3-5]. In ancient times, the roofs of Chinese-architecture houses used a mixture of mud and rice stalks to enhance the bonding strength of the roofs to prevent rain, as shown in Fig. 1.

Therefore, we use rice husk products as reinforcement phase in the thermal spraying industry will have better results.

Thermal spraying is the melting state of powder spraying particles through high-speed air spray atomized spray on the surface of parts. A metal surface finishing process for forming a spray coating. As an important surface engineering technology for new product manufacturing and used product maintenance or remanufacturing, thermal spraying technology has been widely used in aerospace, steel, oil, Marine, military and other fields, such as heat resistance and life extension of turbine blades of aero-engines, corrosion resistance of surface of mechanical parts and so on. NiCrBSi(Ni60) powder, as a self-fusible alloy powder often used in thermal spraying process, has been widely used. However, considering that rice husk products have the

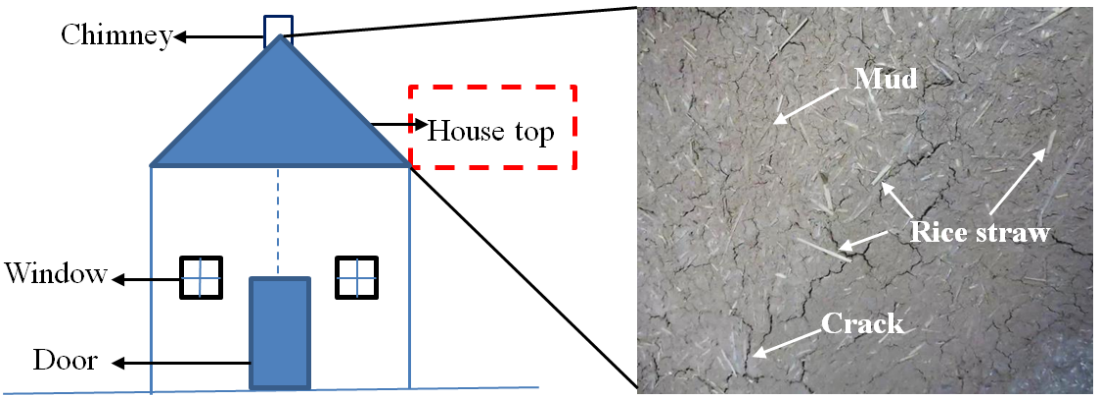

Fig. 1. Sketch of the roofs of Chinese-architecture houses

[1] HENAN LIGHT INDUSTRY VOCATIONAL COLLEGE, ZHENGZHOU, 450002, P.R. CHINA

* Corresponding author: 370818502 @qq.com

characteristics of amorphous fiber, our research group added NiCrBSi(Ni60) as reinforcement phase to the thermal spraying process, whether the bonding strength of the coating could be increased? Therefore, the author did the following work research.

2. Experimental method

2.1. Pyrolysis process of rice husk

Rice husk is a robust protective shell of rice, and it is also a waste in the rice production process. If rice husk, as a biomass energy material shown in Fig. 2a, can be used to transform abundant biomass resources into new types of nanostructure and microstructure materials, the application direction of biomass resources can be further broadened [6,7]. Rice husk has a unique lignocellulose-SiO_2 network structure. As shown in Fig. 2b, it has a unique advantage when synthesizing nanomicrostructured materials. It can be used to synthesize carbon-based materials or silicon-based materials and carbon/silicon composite materials [8,9].

In this study, rice husk was soaked in acetone for 30 min and washed with alcohol to clean the impurities, and then dried in a drying oven at 100°C for 1 h before use.

A synchronous thermal analyzer was used to determine the pyrolysis characteristics of rice husk. Then, 20-mg rice husk powder was put into a crucible, and under the protection of argon, a heating rate of 10°C/min to 900°C/min was selected to obtain a thermogravimetric curve. As shown in Fig. 3, a large area of exothermic peak appeared at about 450°C. This was the result of interleaving and superposition of exothermic peaks of rice husk carbonization. The thermogravimetric curve also dropped sharply. When the time decreased, the temperature difference of the rice husk reaction system increased, and the diffusion effect of the pyrolysis gas in the outer layer of the system was limited, resulting in faster volatilization of the contents of the rice husk, which was not conducive to the pyrolysis of the cellulose inside the rice husk [10].

According to the heating rate of 10°C/min, the kinetic equations of rice husk pyrolysis were evaluated in different pyrolysis stages of rice husk, and mathematical analysis was carried out using the kinetic mechanism function [11,12]. According to the

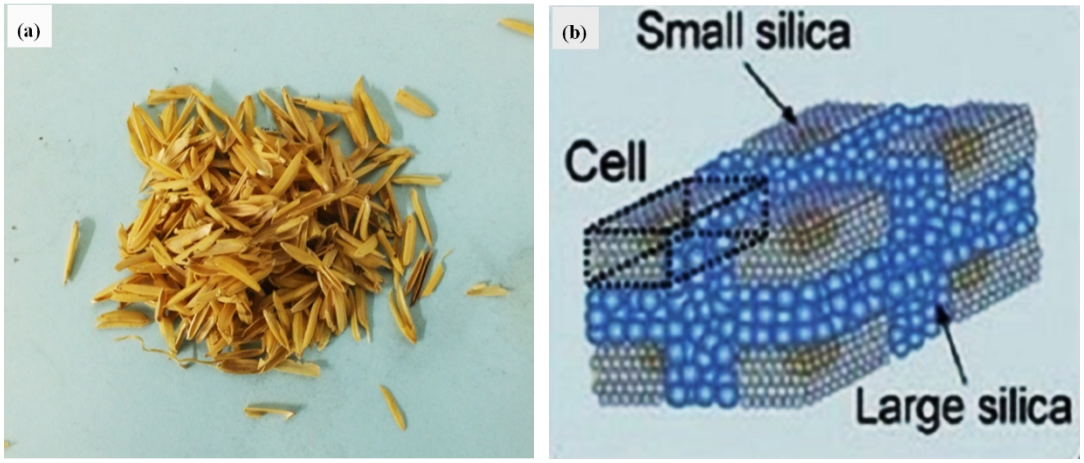

Fig. 2. (a) Photos of rice husk, (b) structural drawings of SiO_2

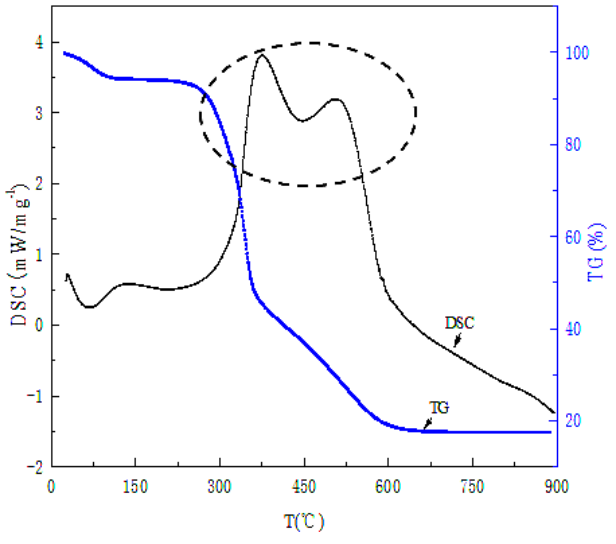

Fig. 3. Pyrolysis curve of rice husk

rate constant K and temperature T, it conformed to the Arrhenius theorem:

$$\left.\begin{aligned} \frac{da}{dt} &= K(T)f(a) \\ K &= A\mathrm{epx}\left(-\frac{E}{RT}\right) \end{aligned}\right\} \tag{1}$$

where A is the frequency factor (min^{-1}); E is the reaction activation energy (kJ/mol); and R = 8.314 J/(mol×K) is the reaction temperature (K). By calculating formula (1) for integration gives:

$$\ln\left[\frac{g(\alpha)}{T^2}\right] = \ln\frac{AR}{\beta E}\left(1-\frac{2RT}{E}\right)-\frac{E}{RT} \tag{2}$$

$$g(\alpha) = \int_0^{\alpha}\frac{d\alpha}{f(\alpha)}, \beta = \frac{dT}{dt}$$

When $\frac{2RT}{E} << 1$,

$$\ln\left[\frac{g(\alpha)}{T^2}\right] = \ln\frac{AR}{\beta E} - \frac{E}{RT} \quad (3)$$

Assuming that the pyrolysis reaction mechanism of rice husk was random nucleation,

$$f(\alpha) = (1-\alpha)^n \quad (4)$$

The pyrolysis reaction of rice husk is regarded as a first-order parallel reaction when n is 1. According to the reference, the kinetic equation obtained was:

$$Y = -484X - 13.12 \quad (5)$$

2.2. XPS curve of rice husk

An x-ray photoelectron spectroscopy (XPS) was performed on the pyrolysis products of rice husk. Fig. 4 shows the XPS spectrum of the pyrolysis products of rice husk. It shows that the product contained only silicon and oxygen. Fig. 4(a) shows one Si 2p binding energy peak. The binding energy of 104.3 eV was the characteristic peak of SiO nanoparticles on the surface of silica, which also indicated that the surface groups of the product were composed of a large amount of phenol and alcohol, carbonyl, and amorphous silica. In Fig. 4(b), two oxygen peaks appeared in O 1s. The O 1s binding energies were 531 eV for 48.3% of oxygen in the carbonyl group and 534.2 eV for 45.5% of alcohol, hydroxyl, and ether [13,14].

2.3. Raw materials and Sample preparation

The pyrolyzed rice husk product was amorphous SiO_2. As shown in Fig. 5(a), the SiO_2 powder was used in a ball mill with a φ5-mm ZrO_2 ball at a rate of 150 rpm, and the grinding time was 5 h to obtain a fiber powder with a length of 40-50 μm. Fig. 5(b) shows the spherical micromorphology of Ni60. The ground SiO_2 and Ni60 powder were mixed in a ratio of 7:3 (wt%), and then mixed in a ball mill at a rate of 100 rpm for 5 h, and 15wt% alcohol was added. As a binder, the uniformly mixed powder was placed in a sealed tank for later use.

A supersonic plasma-spraying equipment was used to spray the mixed powder on the surface of φ10 45# steel substrate. Fig. 6 illustrates a schematic diagram of thermal spraying. The fibrous SiO_2 was light in weight and easy to be blown off by gas during the spraying process, so alcohol was used. As a binder, the

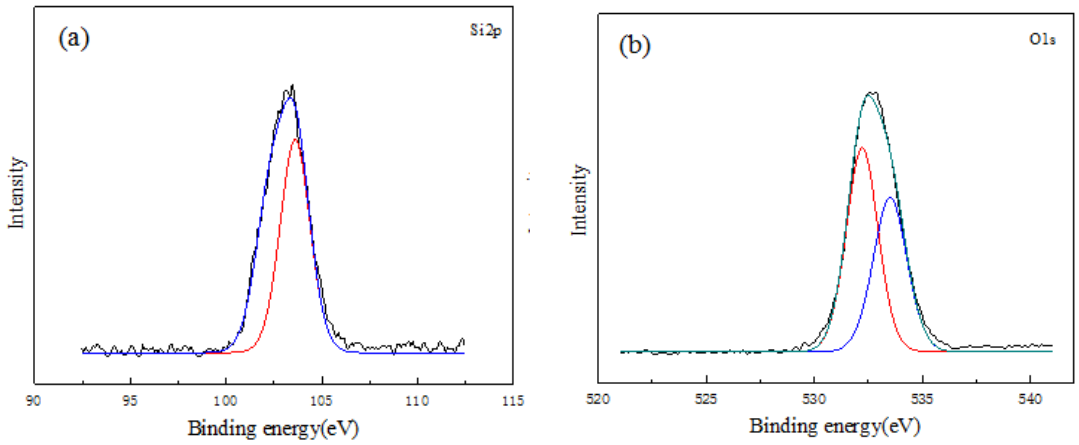

Fig. 4. XPS spectra of rice husk products, (a) Si2p binding energy, (b) O1s binding energy

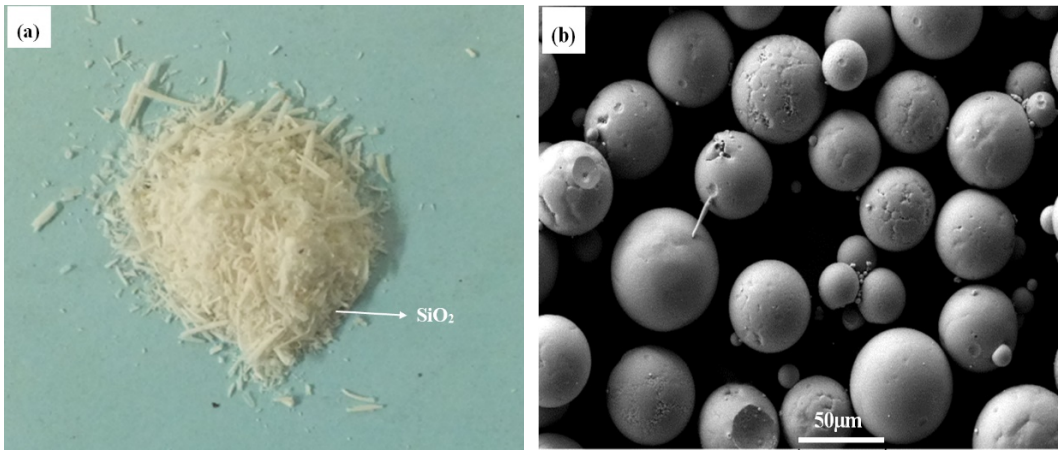

Fig. 5. (a) Powder image of SiO_2, (b) Microscopic morphology of Ni60

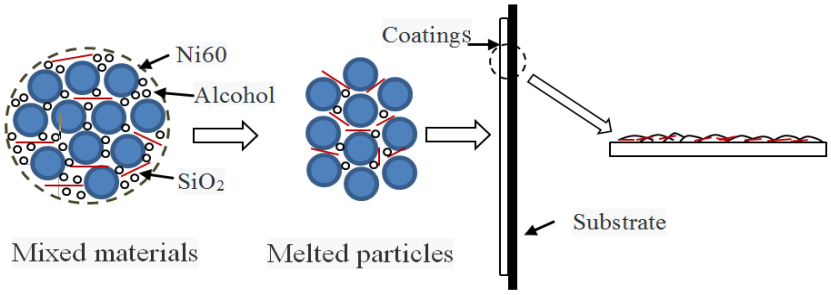

Fig. 6. schematic diagram of Ni60/SiO_2 coating

alcohol volatilized during the thermal-spraying process, fibrous SiO_2 was mixed in Ni60, and then a coating was formed on the surface of the 45# substrate to form the roof structure, as shown in Fig. 1. Next, whether this process enhanced the coating and the performance of the coating were verified.

3. Experimental results and discussion

3.1. Microstructure analysis of the coating

Fig. 7 illustrates the microscopic morphology of the coating. Fig. 7a presents an Ni60/SiO_2-sprayed surface morphology, showing a uniform surface without cracks and inclusions. Fig. 7b is a partial enlarged view, showing SiO_2 fibers in the middle of the coating. Fig. 7c shows the polished surface of the Ni60/SiO_2-sprayed sample. No defects, such as cracks and unmelted particles, and no islands were found on the surface, as shown in Fig. 7d [15].

3.2. XRD analysis of the coating

Fig. 8 shows the phase structure of the Ni60/SiO_2 coating. The Fig. shows six phases, mainly Ni phase, with a fibrous SiO_2 phase. This was also consistent with the SiO_2 fiber attached to the surface in Fig. 7. The coating had a fibrous reinforcement phase and an intermediate phase combining some elements of Ni60 powder, such as Ni3Si2, Cr3Si, Cr5O12, and other phases.

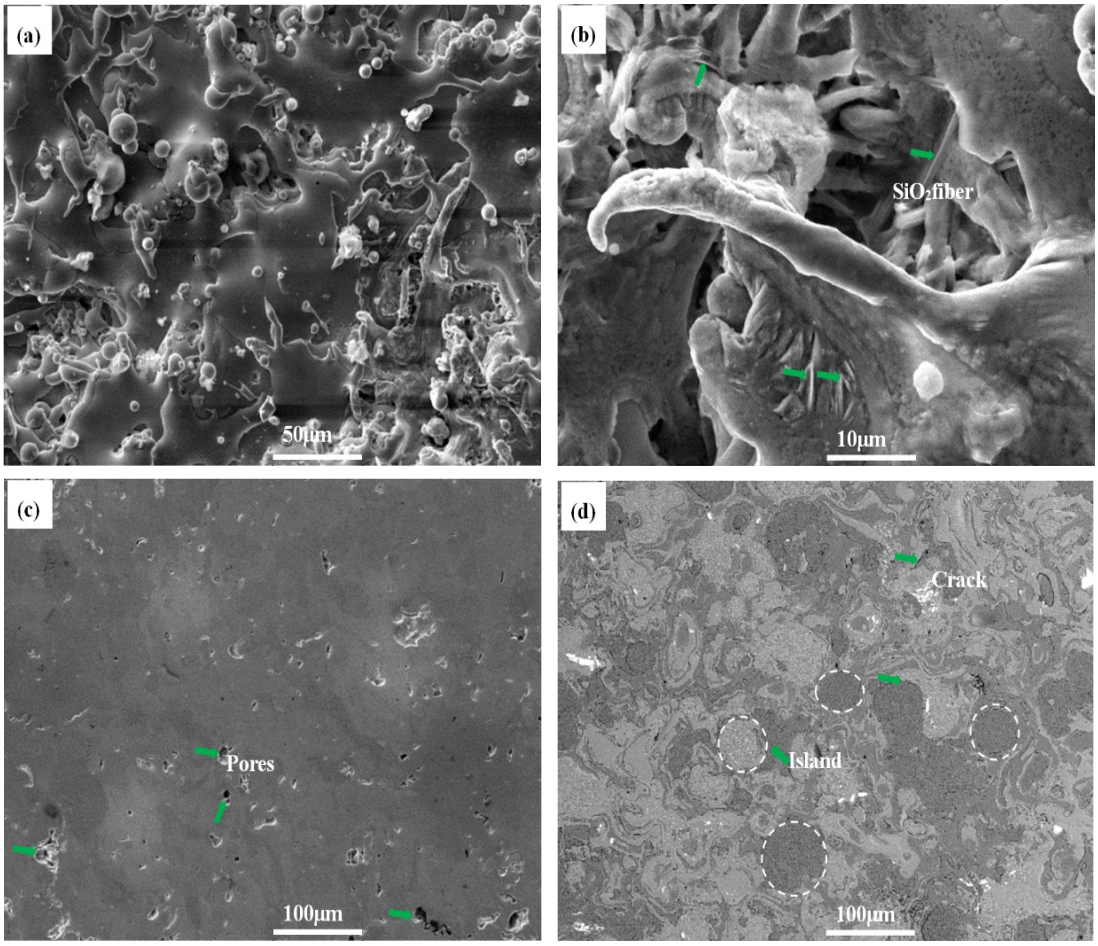

Fig. 7. Microscopic morphology of Ni60/SiO_2 coating, (a) Suface (b) Suface local (c) Polished surface (d) Polished surface of Ni60

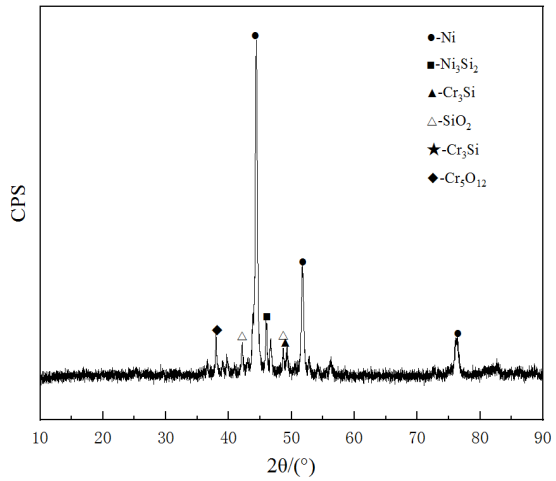

Fig. 8. Phase structure of Ni60/SiO_2 coating

3.3. Hardness and Wear analysis of the coating

The nanoindentation method was used to test the nanoindentation hardness of the coating so as to verify whether the addition of fibrous SiO_2 enhanced the performance of the coating. Fig. 9(a) shows that the loading hardness of the coating surface reached 6506 μN, and the nanoindentation depth reached 138 nm. But in Fig. 9(b), The hardness of the Ni60 coating prepared by the same process was 4695 μN, and the addition of fiber SiO_2 increased the hardness of the coating by 27.8%. Therefore, the enhancement effect was obvious.

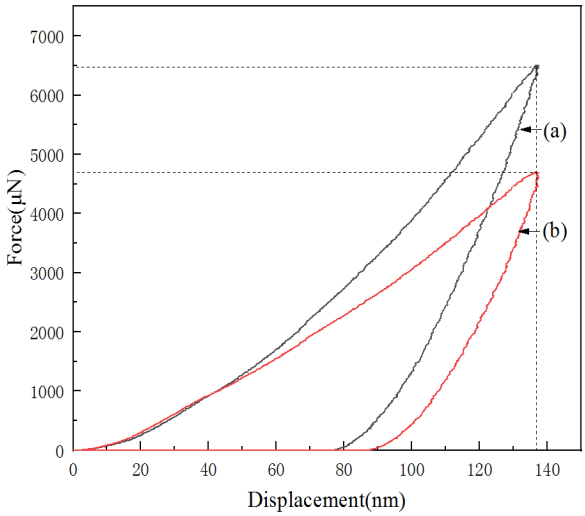

Fig. 9. Hardness of the surface coating, (a) Ni60/SiO_2, (b)Ni60

To improve the hardness of nanoindentation, the Ni60/SiO_2 coating was tested for reciprocating friction and wear, with a friction load of 10 N and friction time of 30 min. Fig. 10 shows that the average friction coefficient of the coating surface was only 0.42, and more irregular burrs were present on the friction coefficient curve, which also reflected the irregular arrangement of SiO_2 fibers in the coating, but it was lower than that of Ni60. The friction coefficient was 0.61, which also reflected that the addition of SiO_2 fiber enhanced the bonding strength of the coating. The 3D wear morphology of Fig. 10 shows that no defects, such as cracks, were observed on the worn surface. The maximum wear depth was 24.5 μm, and the minimum wear depth was 13.3 μm. The surface wear morphology of Fig. 11 shows a furrow shape. The morphology and flaking particles on the surface revealed an abrasive wear mechanism as the cause [16].

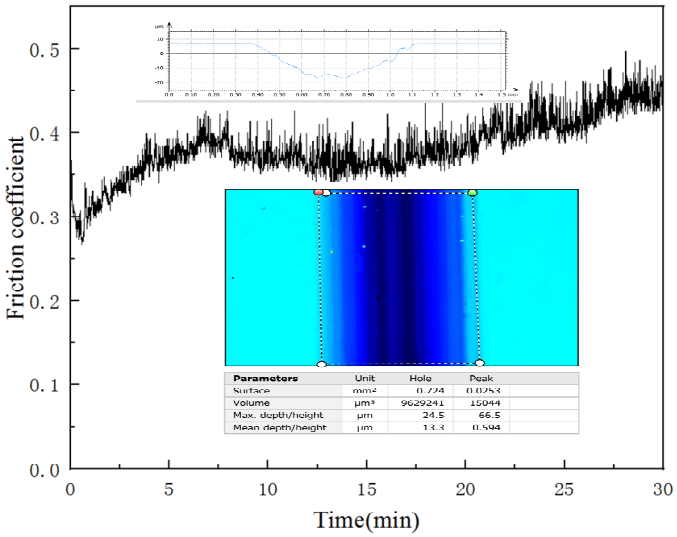

Fig. 10. Friction coefficient and 3D wear morphology of Ni60/SiO_2 coating surface

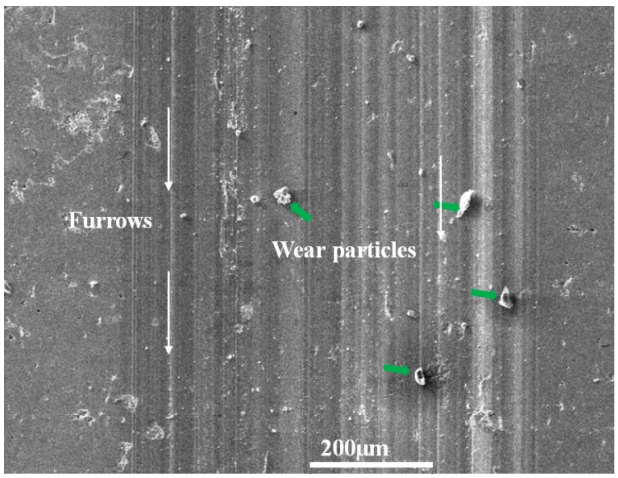

Fig. 11. Surface wear morphology of Ni60/SiO_2 coating surface

4. Conclusions

(1) An Ni60/SiO_2 coating was prepared using a cheap, rice husk pyrolysis product, SiO_2 fiber, as the coating reinforcement phase. The coating had no obvious defects such as cracks and pores.

(2) The nanohardness of the Ni60/SiO_2 coating was 6506 μN, which far exceeded the hardness of the Ni60 coating. Meanwhile, the average friction coefficient was 0.42, which showed that the Ni60/SiO_2 coating had better wear resistance.

(3) Under a load of 10 N, using the reciprocating friction process, the Ni60/SiO_2 coating was mainly manifested as an abrasive wear mechanism.

REFERENCES

[1] Q. Wang, J. Yan, Z. Fan, Carbon materials for high volumetric performance supercapacitors: design, progress, challenges and opportunities, Energ. Environ. Sci. **9** (3), 729-762 (2016). DOI: https://doi.org/10.1039/c5ee03109e

[2] H.B. Feng, H. Hu, H.W. Dong, et al., Hierarchical structured carbon derived from bagasse wastes: A simple and efficient synthesis route and its improved electrochemical properties for high-performance supercapacitors, J. Power. Sources. **302**, 164-173 (2016). DOI: https://doi.org/10.1016/j.jpowsour. 2015.10.063

[3] X.S. Wang, Z.L. Lu, L. Jia, J.X. Chen, Physical properties and pyrolysis characteristics of rice husks in different atmosphere, Results. Phys. **6**, 866-868 (2016). DOI: https://doi.org/10.1016/j.rinp.2016.09.011

[4] B. Marques, J.A. Almeida, A.O. Tadeu, et al., Rice husk cement-based composites for acoustic barriers and thermal insulating layers, J. Build. Eng. **39**, 102297-102313 (2021). DOI: https://doi.org/10.1016/j.jobe.2021.102297

[5] A. Rashad, Cementitious materials and agricultural wastes as natural fine aggregate replacement in conventional mortar and concrete, J. Build. Eng. **5**, 119-141(2016). DOI: https://doi.org/10.1016/j.jobe.2015.11.011

[6] C. Baglivo, P.M. Congedo, High performance precast external walls for cold climate by a multi-criteria methodology, Energy. **115**, 561-576(2016). DOI: https://doi.org/10.1016/j.energy.2016.09.018

[7] Y. Chen, G.E. Okudan, D.R. Riley, Sustainable performance criteria for construction method selection in concrete buildings, Automat.Constr. **19**, 235-244 (2010). DOI: https://doi.org/10.1016/j.autcon.2009.10.004

[8] M. Asim, G.M. Uddin, H. Jamshaid, A. Raza, et al., Comparative experimental investigation of natural fibers reinforced light weight concrete as thermally efficient building materials, J. Build. Eng. **31**, 101411-101422 (2020). DOI: https://doi.org/10.1016/j.jobe.2020.101411

[9] N.A. Liu, K.F. Huo, et al., Rice husks as a sustainable source of nanostructured silicon for high performance Li-ion battery anodes, SCI. Rep-UK. **3**, 1919-1926 (2013). DOI: https://doi.org/10.1038/srep01919

[10] C.M.L. Adrian, Y. Suzana, L.F.C. Bridgid, et al., Comparative study of in-situ catalytic pyrolysis of rice husk for syngas production: Kinetics modelling and product gas analysis, J. Clean. Prod. **197**, 1231-1243 (2018). DOI: https://doi.org/10.1016 /j.jclepro.2018.06.245.

[11] B.L.F. Chin, S. Yusup, P. Kannan, C. Srinivasakannan, S.A. Sulaiman, Comparative studies on catalytic and non-catalytic co-gasification of rubber seed shell and high density polyethylene mixtures, J. Clean. Prod. **70**, 303-314 (2014). DOI: https://doi.org/10.1016/j.jclepro.2014.02.039.

[12] I.Y. Mohammed, Y.A. Abakr, H. Xing, J.N. Alaba, et al., Recovery of clean energy precursors from Bambara groundnut waste via pyrolysis: kinetics, products distribution and optimisation using response surface methodology, J. Clean. Prod. **164**, 1430-1445 (2017). DOI: https://doi.org/10.1016/j.jclepro. 2017.07.068.

[13] Y. Shen, P. Zhao, Q. Shao, In-situ catalytic conversion of tar using rice husk char-supported nickel-iron catalysts for biomass pyrolysis/gasification, Appl. Catal. B-Environ. **152**, 140-151 (2014). DOI: https://doi.org/10.1016/j.apcatb. 2014. 01.032

[14] M.E. Boot-Handford, E. Virmond, N.H. Florin, R. Kandiyoti, P.S. Fennell, Simple pyrolysis experiments for the preliminary assessment of biomass feedstocks and low-cost tar cracking catalysts for downdraft gasification applications, Biomass Bioenerg **108**, 398-414 (2018). DOI: https://doi.org/10.1016/j.biombioe.2017.10.048

[15] X.S. Wang, Z.G. Xing, J.J. Hou, K. Liu, Composite ceramic-Ni60 coating fabricated via supersonic plasma spraying, Chinese. J. Phys. **61**, 72-79 (2019). DOI: https://doi.org/10.1016/j.cjph.2019.08.012

[16] X.S. Wang, Z.G. Xing, Preparation and properties of composite nanoceramic NiCrBSi-TiO2/WC(Co) coatings, Coatings. **10**, 868-879 (2020). DOI: https://doi.org/10.3390/coatings10090868